Available online at www.sciencedirect.com
SCIENCE DIRECT
Polymer 46 (2005) 10925–10935
polymer
www.elsevier.com/locate/polymer

A comparison of reinforcement efficiency of various types of carbon nanotubes in polyacrylonitrile fiber

Han Gi Chae, T.V. Sreekumar[1], Tetsuya Uchida[2], Satish Kumar*

School of Polymer, Textile and Fiber Engineering, Georgia Institute of Technology, Atlanta, GA 30332, USA

Received 28 March 2005; received in revised form 5 August 2005; accepted 30 August 2005
Available online 23 September 2005

Abstract

Polyacrylonitrile (PAN)/carbon nanotubes (CNTs) composite fibers were spun from solutions in dimethyl acetamide (DMAc), using single wall (SWNTs), double wall (DWNTs), multi wall (MWNTs) carbon nanotubes, and vapor grown carbon nanofibers (VGCNFs). In each case, CNT content was 5 wt% with respect to the polymer. Structure, morphology, and properties of the composite fibers have been characterized using X-ray diffraction, Raman spectroscopy, scanning and transmission electron microscopy, tensile tests, dynamic mechanical tests, as well as thermal shrinkage. While all nanotubes contributed to property improvements, maximum increase in modulus (75%) and reduction in thermal shrinkage (up to 50%) was observed in the SWNT containing composites, and the maximum improvement in tensile strength (70%), strain to failure (110%), and work of rupture (230%) was observed in the MWNTs containing composites. PAN orientation is higher in the composite fiber (orientation factor up to 0.62) than in the control PAN fiber (orientation factor 0.52), and the PAN crystallite size in the composite fiber is up to 35% larger than in the control PAN (3.7 nm), while the overall PAN crystallinity diminished slightly. Nanotube orientation in the composite fibers is significantly higher (0.98 for SWNTs, 0.88 for DWNTs, and 0.91 for MWNTs and VGCNFs) than the PAN orientation (0.52–0.62). Improvement in low strain properties (modulus and shrinkage) was attributed to PAN interaction with the nanotube, while the improvement in high strain properties (tensile strength, elongation to break, and work of rupture) at least in part is attributed to the nanotube length. Property improvements have been analyzed in terms of nanotube surface area and orientation.

Keywords: Carbon nanotube; Polyacrylonitrile; Carbon fiber

1. Introduction

Carbon fibers developed since 1960s are now widely used in composite applications. Vapor grown carbon nano fibers (VGCNFs) developed in 1980s [1], and carbon nanotubes (single wall—SWNTs [2,3], double wall—DWNTs [4,5], and multiwall—MWNTs [6]) developed in 1990s have exceptional physical, mechanical, electrical, thermal, and optical properties [7,8] and are sometimes heralded to be the ultimate reinforcing systems for polymer and other matrices. Significant breakthroughs have been reported in processing carbon nanotubes [9–11] and carbon nanotube/polymer composite films [12–18] and fibers [19–21]. Pristine or functionalized [22–28] carbon nanotubes have been dispersed in more than 25 polymer matrix systems, including semi-crystalline [29,30] and amorphous [31,32] thermoplastics, thermosetting polymers [33,34], water soluble polymers [35], liquid crystalline polymers [20,36], and conjugated polymers [37,38]. Carbon nanotubes are also being used to reinforce ceramics [39–41] and metal matrices [42–44]. Property improvements with carbon nanotubes include enhanced tensile modulus [45–47], tensile strength [47–49], torsional modulus [50], compressive strength [51,52], fatigue behavior [53], toughness [47], glass transition temperature [47,54–56], electrical conductivity [57,58], thermal conductivity [17,59], solvent resistance [47,60,61], and reduction in thermal shrinkage [47,51,56], as well as anisotropic optical properties [47]. Carbon nanotube based materials are also being evaluated for their functional characteristics, such as charge storage device [62–64], field emission [65–67], sensors of chemical [68,69], stress [70], and temperature [71,72]. Carbon nanotubes are being dispersed in polymer matrices using organic solvents, or aqueous media with the aid of surfactant [73,74], in situ polymerization [20], as well as in melt [75]. While poly(vinyl alcohol) (PVA) [13,19,76], poly(methyl methacrylate)

* Corresponding author. Tel.: +1 404 894 7550.
E-mail address: satish.kumar@ptfe.gatech.edu (S. Kumar).
[1] Current address: DMSRDE, Kanpur 208 013, India.
[2] Current address: Faculty of Engineering, Okayama University, Okayama 700-8530, Japan.

0032-3861/$ - see front matter © 2005 Elsevier Ltd. All rights reserved.
doi:10.1016/j.polymer.2005.08.092

(PMMA) [50,77], and epoxy [78,79] based composites received early attention and perhaps remain the most studied polymer/CNT systems to date, polyacrylonitrile/CNT composites are turning out to be quite important [47,60,62,80–89]. Polyacrylonitrile is a commercially important polymer [90] and is the predominant precursor for carbon fibers [91]. PAN/CNT films and fibers with significant property improvements are being processed [47,62,84,85] from solutions in dimethyl formamide or in dimethyl acetamide, suggesting good interaction between polyacrylonitrile and carbon nanotubes, and the preliminary stabilization [86] and carbonization studies [87] on PAN/CNT composites have been reported. Which type of carbon nanotube will have the best reinforcement efficiency? This question has received little attention to date [92], and there are no reported fiber studies, comparing the reinforcement efficiencies of different types of nanotubes. Here, the reinforcement efficiency of SWNTs, DWNTs, MWNTs, and VGCNFs has been compared in polyacrylonitrile fiber at 5 wt% nanotube content.

2. Experimental

PAN (molecular weight 100,000 g/mol) obtained from Japan Exlan Co. Ltd. was dried in vacuo at 90 °C. SWNTs were obtained from Carbon Nanotechnologies, Inc. (Houston, TX), DWNTs from Nanocyl, Co. (Belgium), MWNTs from Iljin Nanotech, Co. (Korea), and VGCNFs (PR-24-HT, heat treated at 2850 °C) from Applied Sciences, Inc. (Cedarville, OH). The amount of catalytic impurity in each type of nanotube was estimated from the thermogravimetric analysis (TGA) under air based on the residual weight [93]. Based on this analysis, the impurity was 2.4, 5.4, 2.5, and 0.3 wt% in SWNT, DWNT, MWNT, and VGCNF, respectively. *N*,*N*-dimethylacetamide (DMAc) was obtained from Sigma–Aldrich, Co. and was used as received. CNTs (1.5 g) were dispersed in 300 mL DMAc using simultaneous sonication (Cole–Parmer 8891R-DTH, 80 W, 43 kHz) and stirring, until dispersion reached optical homogeneity. SWNTs, MWNTs, and VGCNFs formed optically homogeneous dispersion in less than 10 h of sonication, while highly entangled DWNTs required continuous sonication for 2 weeks before optically homogenous dispersion could be obtained. 28.5 g PAN was separately dissolved in 150 mL DMAc at 70 °C, and PAN/DMAc solution was added to the CNT/DMAc dispersion and homogenized while stirring. Excess solvent was evaporated to obtain the desired solution concentration of 30 g solids (PAN + CNT) in 150 mL DMAc. Accounting for impurity, CNT content, in each case was 5 ± 0.3 wt% with respect to the weight of the polymer.

The PAN/CNT/DMAc solutions were spun at room temperature by dry-jet-wet spinning using the small scale spinning system manufactured by Bradford University Research Ltd. The air gap between spinneret (single hole, 500 μm diameter) and the coagulation media was about 2 cm. The schematic of the spinning set up is shown in Fig. 1. A 635 mesh (20 μm) stainless steel filter pack (TWP, Inc.) was used in the spinning line. DMAc/water volumetric ratios in the coagulation baths (baths 1 and 2) and drawing bath (bath 3) were 60/40, 10/90, and 0/100, respectively, while the two coagulation baths were maintained at 30 °C and the drawing bath at 100 °C. An in-line heater was used for fiber drying and was maintained at 130 °C. There was no fiber drawing in the two coagulation baths. Fiber was drawn between 1st and 2nd rollers, and fibers were allowed to relax and dried in the heating block. Take-up roller speed was set to be a little lower (19.4 m/min) than the 2nd roller speed (20 m/min). The final draw ratio of the control PAN and for each composite fiber was 10. The fibers were further dried in a convection oven at 50 °C for 1 week at constant length.

Fiber mechanical properties were determined using RSA III solids analyzer (Rheometric Scientific, Co.). The gauge length and crosshead speed for the tensile tests were 25 mm and 0.1 mm/s, respectively. For tensile tests, at least 10 filaments were tested in each case. Dynamic mechanical tests were conducted at 10 Hz at a heating rate of 2 °C/min, and on bundles of 10 filaments at 25 mm gauge length. Thermal shrinkage was determined using thermo-mechanical analyzer (TMA 2940, TA Instruments) at 15 MPa pre-stress in the extension mode at a heating rate of 10 °C/min. Raman spectra were collected in the back scattering geometry using a Holoprobe Research 785 Raman Microscope made by Kaiser Optical System using 785 nm excitation laser with polarizer and the analyzer parallel to each other. Spectra were collected when the fiber axis was at 0, 5, 10, 20, 30, 40, 50, 60, 70, 80, 85, and 90° from the polarization direction. The SWNTs and DWNTs orientation in the composite fiber was determined

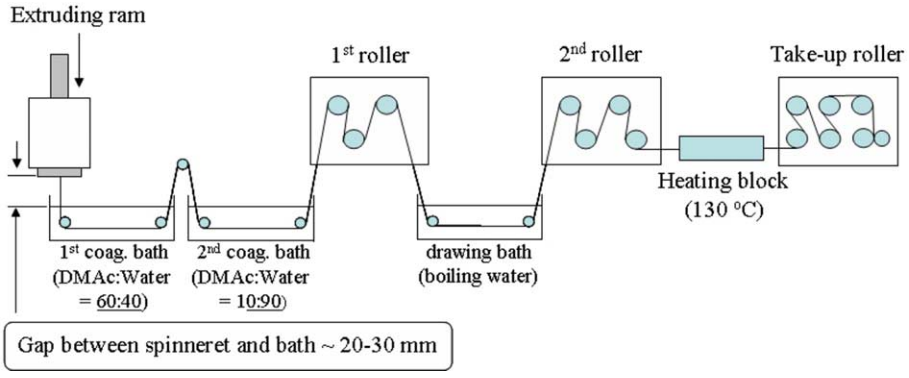

Fig. 1. Schematic diagram of the dry-jet-wet fiber spinning set up.

from the peak intensity of tangential band (ca. 1590 cm^{-1}) assuming Gaussian intensity distribution with respect to the polarization direction [94]. The orientation of MWNTs in the composite fiber was determined from the graphite (002) azimuthal scan obtained from X-ray diffraction. From the orientation factor of the graphite plane normal, −0.455, orientation factor of the graphite plane was determined to be 0.91 on the assumption of the symmetry of orientation along the *a* and *b* axes. The orientation of the VGCNF was also determined from the graphite (002) azimuthal scan. The graphitic layers in VGCNFs make an angle of 15° to the fiber axis [95]. Therefore, to determine the orientation of VGCNFs, the azimuthal scan profile was fitted by two Gaussian peaks, with peak positions located at ±15° around the equator as described elsewhere [95]. Wide angle X-ray diffraction (WAXD) patterns were obtained on multifilament bundles by Rigaku Micromax-007 (operated at 45 kV, 66 mA, $\lambda = 1.5418$ Å) using Rigaku R-axis IV++ detection system. The diffraction patterns were analyzed using AreaMax V. 1.00 and MDI Jade 6.1. PAN orientation was determined from the (200,110) azimuthal scans ($2\theta = 16.7°$) using the previously described procedure [47]. PAN crystallinity was determined by area-calculation of deconvoluted integrated diffraction patterns [96–98]. In PAN/MWNTs and PAN/VGCNFs composite fibers, the graphite peak was also present and was excluded from the PAN crystallinity calculation. The PAN crystal size was determined from the peak at $2\theta = 16.7°$ using the Scherrer equation with $K = 0.9$ [99]. Fiber tensile fractured surfaces were observed on the gold coated samples by scanning electron microscopy (LEO 1530 SEM operated at 15 kV). Transmission electron microscopy (TEM) specimens for the composite fibers were prepared by detachment method using parlodian [100]. Bright field TEM images were recorded on Mitsubishi Microscope Film using JEM 2000EX (operated at 200 kV).

3. Results and discussion

Fig. 2 shows the bright field TEM images of various nanotubes used in this study. As expected, SWNTs show 5–50 nm diameter bundles or ropes, with an average diameter of about 30 nm. Diameters of DWNTs were about 5 nm, and they mostly existed as individual tubes, however, these were highly entangled. The average diameter of MWNTs was about 20 nm, and these also existed as mostly individuals, though entangled. Diameter of vapor grown carbon nano fibers was about 60 nm and they appeared to be relatively free of entanglements. As mentioned in the experimental section, DWNTs, due to high degree of entanglement, were the most difficult to disperse. By comparison SWNTs and MWNTs were readily dispersed by sonication, suggesting a relatively less entangled structure in these two types of nanotubes. TGA plots indicate that SWNT, DWNT, MWNT, and VGCNF degradation peaks in air at about 500, 440, 600, and 700 °C, respectively (Fig. 3(A)). Degradation in MWNT and VGCNF is delayed due to the existence of the layered graphitic structure in these. For comparison, thermogravimetric analysis results in nitrogen (Fig. 3(B)) show that all nanotubes do exhibit degradation in the 800–1000 °C range. SWNT exhibit the most degradation followed by DWNT, MWNT, and VGCNF. Raman spectra (Fig. 4) show that the intensity of the disorder band (ca. 1300 cm^{-1}) in MWNTs and in VGCNF is quite high, suggesting highly defective graphitic structure in these two cases. Among the four types of tubes, SWNTs appear to have the highest perfection followed by DWNTs.

Mechanical properties and various structural parameters for the control PAN and the composite fibers are listed in Table 1. All composite fibers exhibit improved mechanical properties over the control PAN. Increase in modulus and decrease in shrinkage is the highest in SWNT containing fibers, while

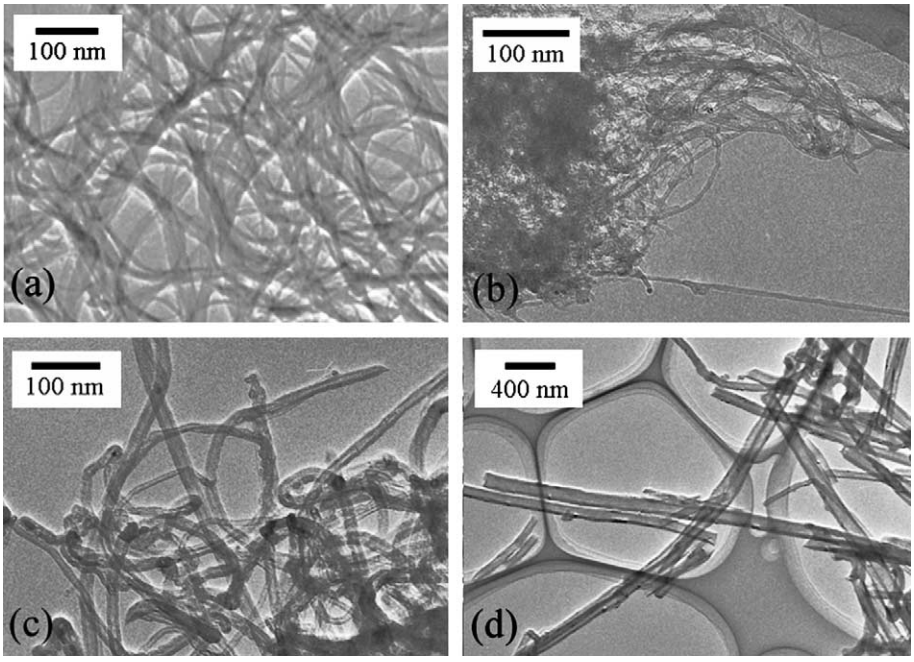

Fig. 2. Bright field TEM images of carbon nanotubes used in this study: (a) SWNTs, (b) DWNTs, (c) MWNTs, and (d) VGCNFs.

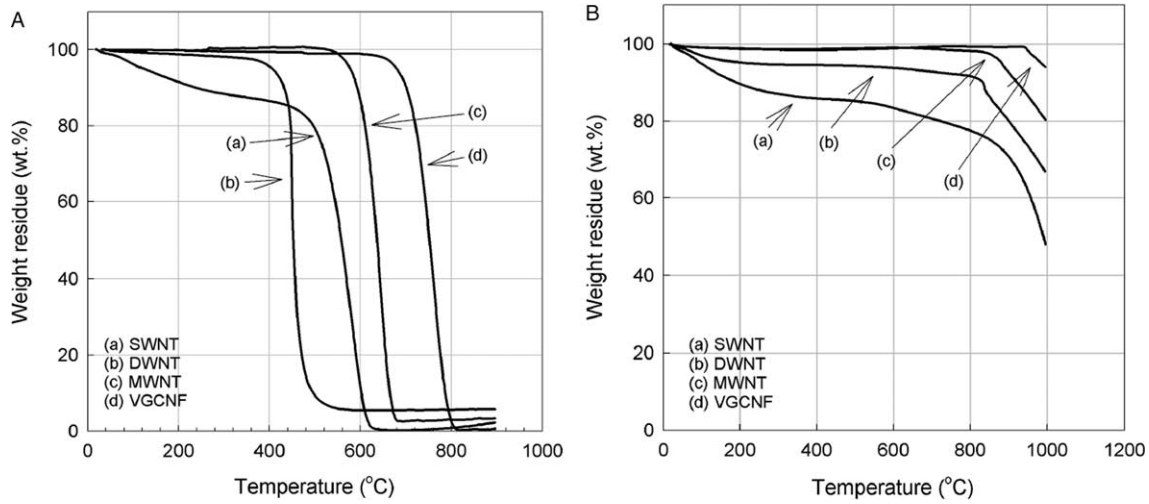

Fig. 3. Thermogravimetric analysis plots of (a) SWNTs, (b) DWNTs, (c) MWNTs, and (d) VGCNFs powder at a heating rate of 10 °C/min in (A) air and (B) nitrogen.

increase in tensile strength, strain to failure, and toughness was the highest in MWNTs containing fibers. Improvement in all the properties in PAN/DWNTs and PAN/VGCNFs composite fibers was intermediate to that of PAN/SWNTs and PAN/MWNTs. While conventional fillers and reinforcements improve modulus and strength at the expense of strain to failure and toughness, all nano carbon reinforcements used in this study improved all mechanical properties, including up to 230% improvement in fiber toughness (with just 5 wt% MWNTs) as measured from the area under the stress–strain curve.

Storage modulus at 140 °C is enhanced by almost a factor of 6 (for SWNT containing fibers), while the tan δ peak temperature increased from 100 °C for the control PAN to 109 °C for the PAN/SWNTs composite, and the magnitude of the tan δ peak decreased from >0.3 for the control PAN to below 0.2 for the composite fibers (Fig. 5). Storage moduli in the entire temperature range for the MWNT and VGCNF containing composite fibers were quite comparable to each other. On the other hand, the storage modulus of the composite containing DWNT was substantially higher than that of the control fiber, above the glass transition temperature, while it only exhibited a moderate increase at room temperature. Width of the tan δ vs temperature plot for the composite fibers (except SWNT containing fibers) is significantly reduced as compared to that of the control PAN. This suggests a narrower spectrum of relaxation times in the composites than in PAN, a result of polymer interaction with the nanotubes. In the case of SWNT containing fibers, tan δ peak is broadened towards high temperature. We conjecture that PAN interactions with SWNT are stronger than with other larger diameter nanotubes, and that PAN segments closer to the SWNT exhibit tan δ loss at higher temperature than the segments farther from it, leading to the broadening in the high temperature region. Intercalation of PAN in the SWNT bundle may also be partially responsible for the tan δ broadening behavior.

SWNT containing fibers exhibited most improvement in the thermal shrinkage behavior, followed by MWNTs, VGCNF, and DWNT, respectively (Fig. 6). In the control PAN fiber, as there are no nanotubes, amorphous chains are free to relax, unless constrained by the crystalline regions. In the PAN–CNT composite, due to polymer nanotube interaction, an additional constraint is imposed on the PAN molecules, resulting in improved thermal shrinkage performance. DWNT containing samples exhibit poor performance due to high degree of entanglement and agglomeration. Under comparable spinning conditions, PAN orientation factors in the composite fibers were 0.62, 0.60, 0.57, and 0.53 for SWNT, MWNT, VGCNF, and DWNT containing fibers, while the orientation of the control PAN fiber was 0.52. All types of CNTs, including VGCNF, resulted in enhanced polymer orientation, with SWNT resulting in most enhancements. Normally fibers with high degree of orientation results in large thermal shrinkage, and unoriented fiber would exhibit no entropic shrinkage. Considering that the nanotube containing fibers exhibit higher orientation than

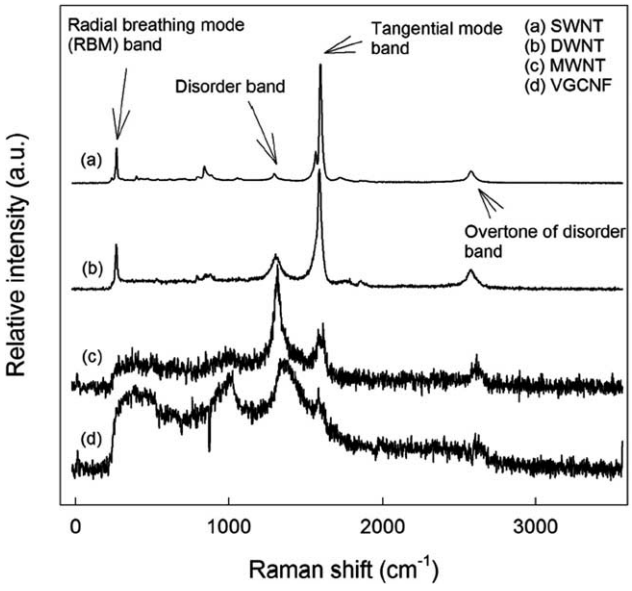

Fig. 4. Raman spectra for pristine (a) SWNTs, (b) DWNTs, (c) MWNTs, and (d) VGCNFs powder.

Table 1
Structural parameters and properties of control PAN and PAN/CNT composite fibers

	Control PAN	PAN/SWNTs	PAN/DWNTs	PAN/MWNTs	PAN/VGCNFs
Modulus (GPa)	7.8±0.3	13.6±0.5	9.7±0.5	10.8±0.4	10.6±0.2
Strength at break (MPa)	244±12	335±9	316±15	412±23	335±13
Strain to failure (% strain)	5.5±0.5	9.4±0.3	9.1±0.7	11.4±1.2	6.7±0.3
Toughness (MPa)	8.5±1.3	20.4±0.8	17.8±1.7	28.3±3.3	14.0±1.0
Shrinkage at 160 °C (%)	13.5	6.5	11.5	8.0	11.0
T_g [a] (°C)	100	109	105	103	103
f_{PAN}	0.52	0.62	0.53	0.60	0.57
f_{CNT}	–	0.98	0.88	0.91	0.91
Crystal size (nm)	3.7	5.0	4.1	5.0	4.4
Crystallinity (%)	58	54	57	55	55

[a] tan δ peak temperature.

the control PAN, the reduction in their thermal shrinkage conveys stronger PAN–CNT interaction than if the PAN orientation in the composite was the same as in the control PAN.

Integrated radial WAXD scans, including the deconvoluted scans and the flat plate photographs for various fibers are given in Fig. 7. The crystallinity of the control PAN fiber was only marginally higher than that of the composite fibers. However, PAN crystal size obtained from (200,110) peak, was larger in all composite fibers, and 35% larger in SWNT and MWNT containing fibers than the control PAN. As was the case with

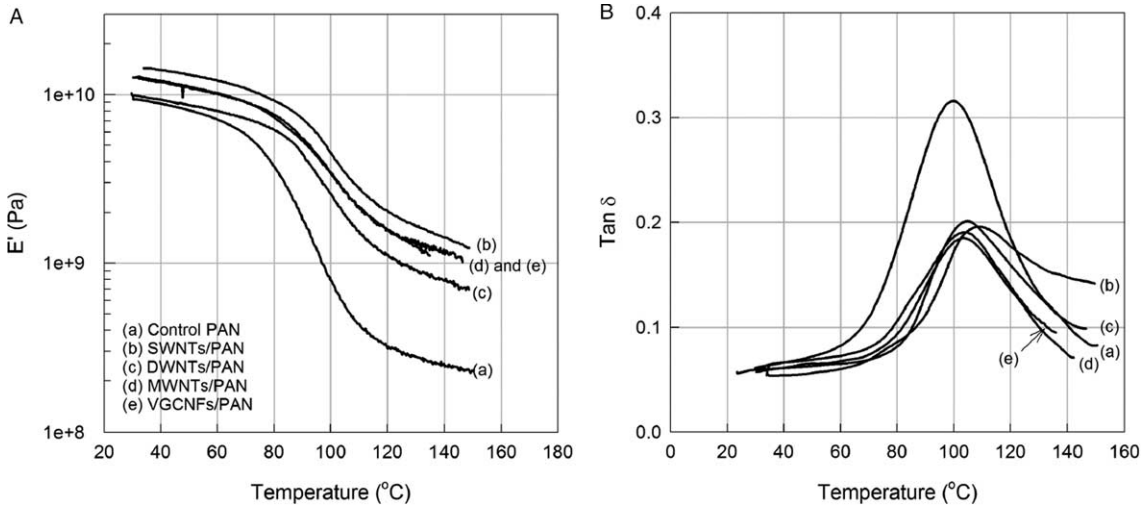

Fig. 5. (A) Storage modulus and (B) tan δ vs temperature plots of various composite fibers.

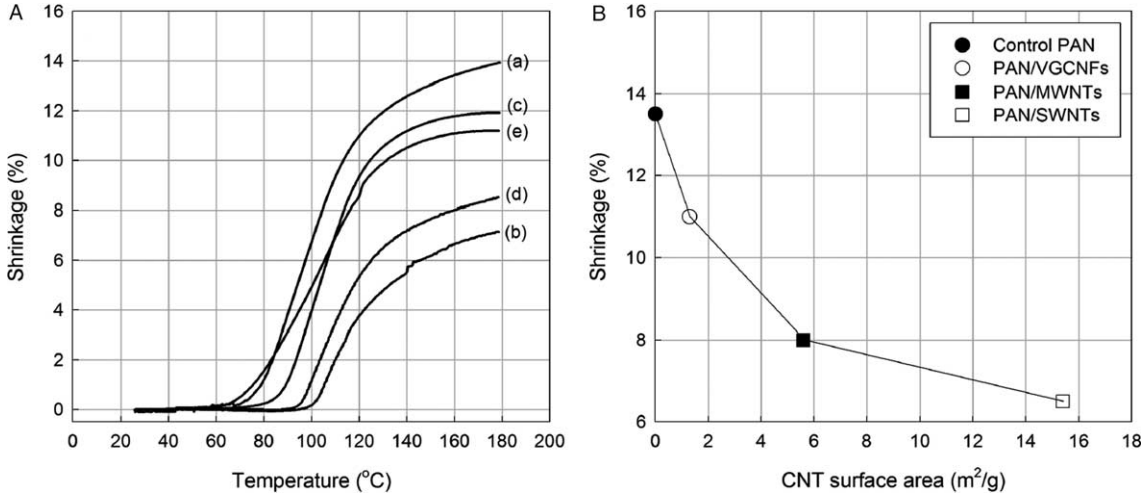

Fig. 6. (A) Thermal shrinkage in various fibers as a function of temperature. Figure legend same as in Fig. 5(A). (B) Thermal shrinkage in various fibers at 160 °C as a function of CNT surface area.

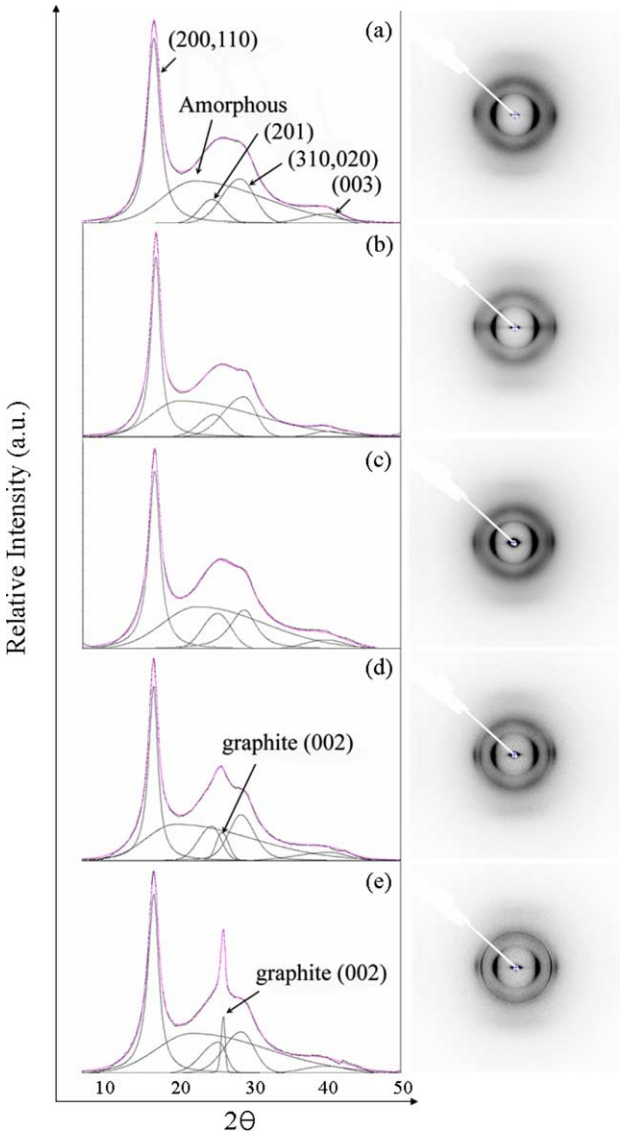

Fig. 7. WAXD patterns, integrated radial scans and the deconvoluted profiles for (a) control PAN, (b) PAN/SWNTs, (c) PAN/DWNTs, (d) PAN/MWNTs, and (e) PAN/VGCNFs.

orientation, composite fiber containing DWNTs exhibited the smallest increase in crystal size. PAN is currently the predominant precursor for carbon fibers. Stabilization and carbonization studies on PAN/carbon nanotubes composites point to the potential of this composite system as a precursor for next generation carbon fiber [86,87]. Fibers with larger PAN crystals and higher polymer molecular orientation are expected to lead to a more perfect and higher orientation carbon fiber with improved mechanical properties.

Tensile fractured surfaces reveal fibrillar structure in both the control PAN and the PAN/CNTs composite fibers (Fig. 8). Many more fibril ends are observed in PAN/SWNT fiber than in PAN/MWNT fiber. SWNT bundles are known to be wrapped by PAN molecules [60,62], and we suggest that the fibril ends observed in PAN/SWNT composite are PAN wrapped SWNTs bundles (Fig. 8(b)). The fact that numerous fibril ends are visible in PAN/SWNT than in PAN/MWNT, suggests that SWNT or SWNT bundles are much shorter than MWNTs. Higher tensile strength and higher toughness of the PAN/MWNT fiber, over that of the PAN/SWNT fiber is attributed to longer MWNTs than SWNTs. This behavior is analogous to the increased tensile strength with increasing molecular weight in polymers [101–104].

Bright field TEM images of thin peeled composite fibers as well as the schematics showing the presence of carbon nanotubes are shown in Fig. 9. SWNTs, MWNTs, as well as VGCNFs are mostly oriented along the fiber axis. However, these are not quite straight, as kinked, bent, and curved nanotubes were generally observed. SWNT bundle diameter in the composite fiber is about 10 nm [105]. This represents partial exfoliation of the SWNT bundles, as the diameter of the SWNT ropes in the powder used in this study was about 30 nm. SWNT, MWNT, and VGCNF agglomeration was not observed in these composite fibers. Occasionally MWNTs with orientation perpendicular to the fiber axis were also observed. SWNT bundles were typically 100–300 nm long (Fig. 9(a)), while MWNTs longer than 1 μm were often observed (Fig. 9(c)). VGCNFs also survived the sonication and fiber processing conditions, and were also typically longer than 1 μm. However, due to the stacked cup geometry [92,106], the strength of the VGCNF is lower than that for the MWNTs, resulting in lower tensile strength improvement in PAN/VGCNF than in PAN/MWNT. In PAN/DWNT composite fiber, the dispersed nanotubes were mostly individuals and well oriented. However, TEM images also reveal the presence of entangled and unoriented DWNTs globules (Fig. 9(b)). The limited property improvements in PAN/DWNT composite fibers are a result of the presence of these unoriented and entangled DWNT globules. The size of these DWNT globules is in the range of 50–200 nm, which is below the resolution limit of the optical microscope and explains why solutions containing such globules appeared to be mostly optically homogeneous.

The enhancements in tensile and dynamic mechanical properties as well as reduced thermal shrinkage, all point to interaction between carbon nanotubes and the PAN matrix. The question is what factors are responsible for different levels of property improvements with different nanotubes. Low strain properties (modulus and thermal shrinkage) were most improved in PAN/SWNT, while high strain properties (tensile strength, strain to failure, and toughness) were most improved in PAN/MWNT. As addressed above, the improvements in high strain properties are a result of longer MWNT than SWNTs. The improvements in low strain properties are dominated by the polymer/CNT interaction, which will depend on the interface area. Strength of the interaction may also depend on the nanotube curvature, as due to higher non planar strains arising from pyramidization of the conjugated carbon atoms and π-orbital misalignment between adjacent pairs of conjugated carbon atoms [107,108], smaller diameter tubes would provide stronger interaction than the larger diameter tubes. This would favor

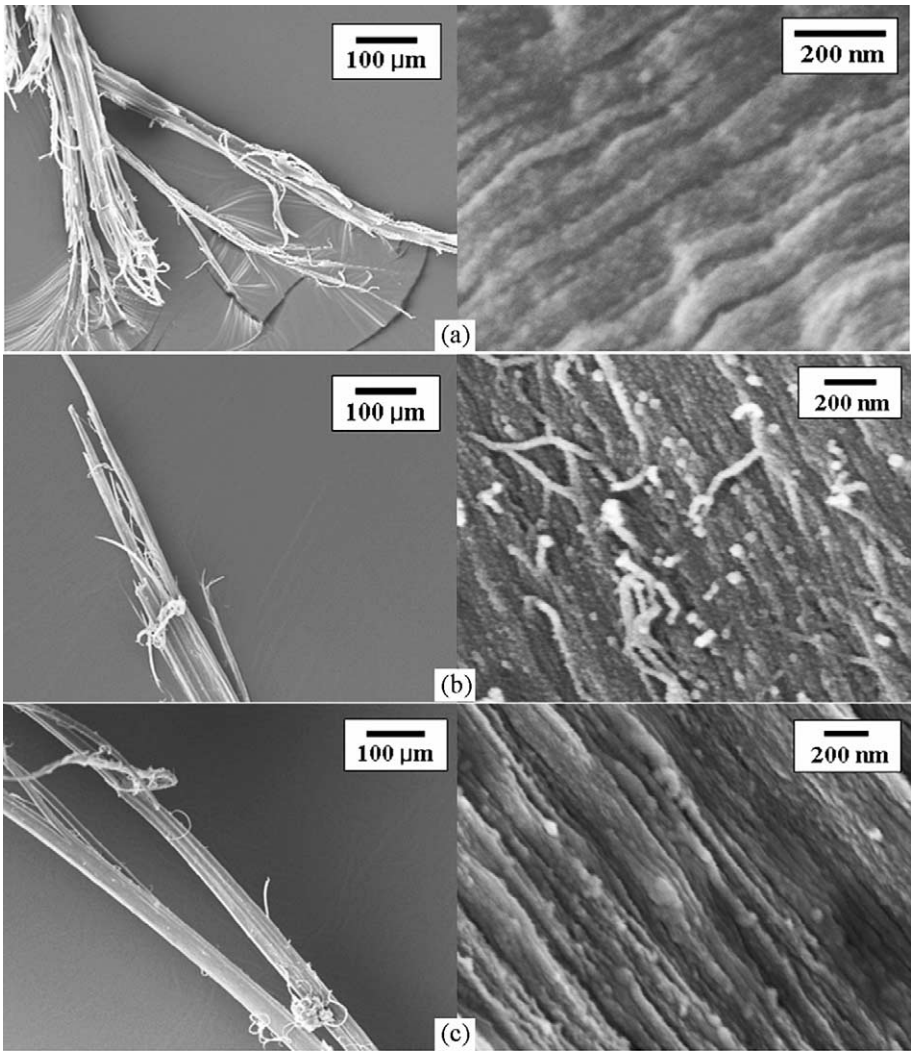

Fig. 8. SEM images of the tensile fractured surfaces; (a) control PAN, (b) PAN/SWNTs, and (c) PAN/MWNTs fibers.

SWNTs over DWNTs and MWNTs. At 5 wt% nanotube loading, the calculated polymer/CNT interface area for various types of nanotubes along with their diameters and densities are listed in Table 2. The trend of the interface area for SWNTs (10 nm diameter bundle) > MWNTs > VGCNFs is in qualitative agreement with the reduction in thermal shrinkage (Fig. 6(B)). The interface area for the DWNTs is higher than that of the SWNT bundles (10 and 20 nm diameter), however, as mentioned earlier, the PAN/DWNT composite fiber contained DWNT globules, which limited the property improvements in this system. Based on the TEM observations, the length of the dispersed DWNTs in the composite fiber was comparable to the length of the SWNT bundles. Considering the fact that DWNTs were sonicated for nearly 2 weeks as opposed to 10 h of sonication for SWNTs, suggests that DWNTs were originally much longer than SWNTs, leading to greater degree of entanglement for the former. The interface area calculations further suggest that well dispersed DWNTs (surface area 26.6 m^2/g at 5 wt% DWNTs) and well dispersed and fully exfoliated SWNTs (surface area 154 m^2/g at 5 wt% SWNTs) would lead to further enhancement in modulus and other low strain properties such as thermal shrinkage, glass transition temperature, as well as modulus improvement above the glass transition temperature. Retention of the SWNT and DWNT length would also lead to further improvements in the high strain properties (strength, strain to failure, and toughness).

Modulus of the composite films and fibers depends significantly on the nanotube orientation and exfoliation [109]. Modulus of the composite fiber was estimated using the following equation:

$$E_{\text{composite}} = (E_{\text{PAN}})_{\text{comp}} V_{\text{PAN}} + (E_{\text{CNT}})_{\text{II}} V_{\text{CNT}} \quad (1)$$

where, $(E_{\text{PAN}})_{\text{comp}}$, $(E_{\text{CNT}})_{\text{II}}$ are the moduli of the two components along the fiber axis, and V_{PAN}, and V_{CNT} are their volume fractions. $(E_{\text{PAN}})_{\text{comp}}$ for each composite fiber was estimated based on the modulus of the control PAN as well as the PAN orientation in the control PAN and in the respective composite fiber. Effective $(E_{\text{CNT}})_{\text{II}}$ for SWNT, and MWNT along the composite fiber axis was calculated using the following continuum mechanics equation [110], as described

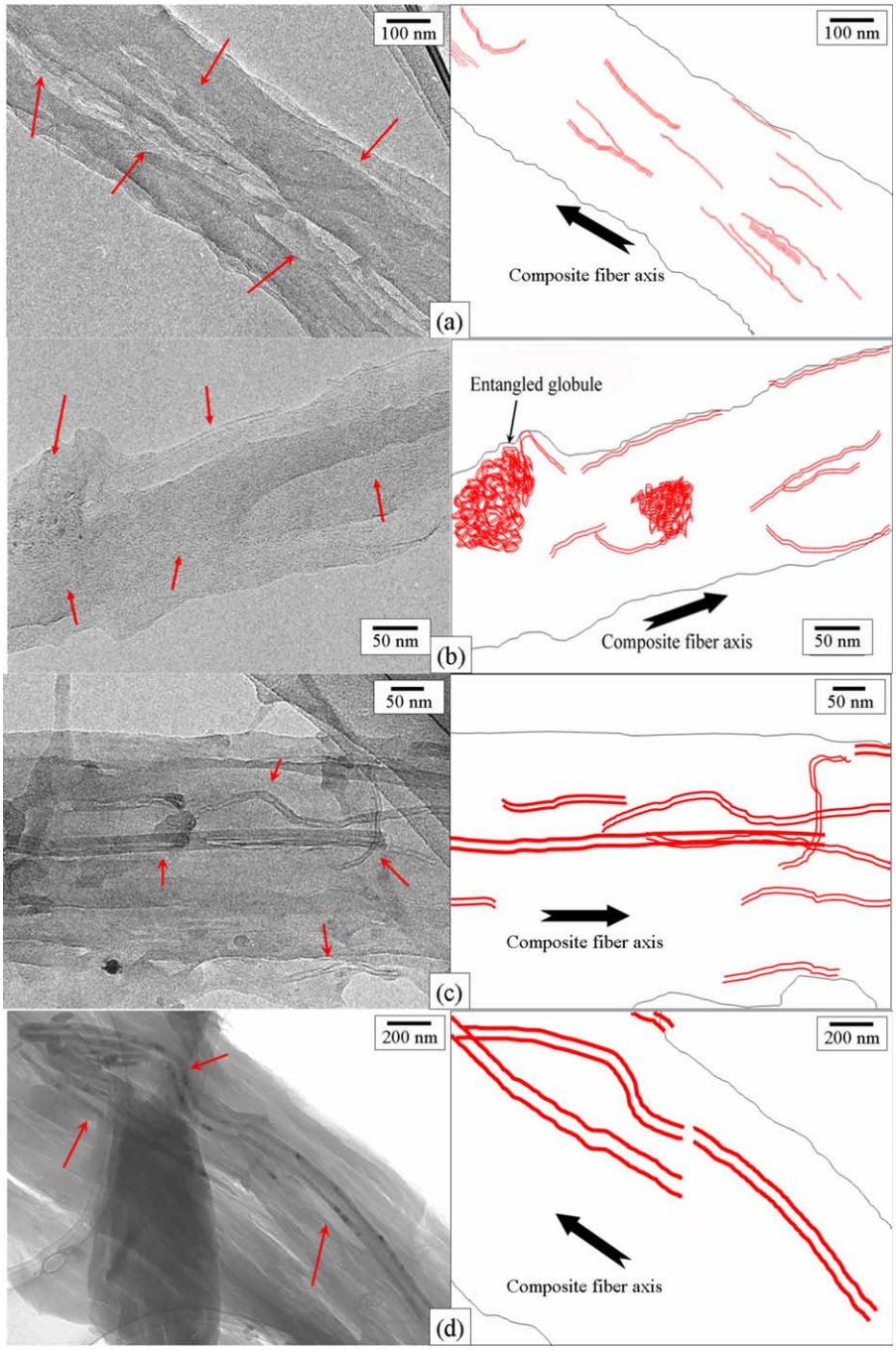

Fig. 9. Bright field TEM images and the schematics showing the presence of carbon nanotubes in various composite fibers; (a) PAN/SWNTs, (b) PAN/DWNTs, (c) PAN/MWNTs, and (d) PAN/VGCNFs.

elsewhere [47,109]:

$$\begin{aligned}\frac{1}{(E_{CNT})_{II}} &= \frac{1}{E_1}\langle\cos^4\theta\rangle + \frac{1}{E_2}\langle\sin^4\theta\rangle + \left(\frac{1}{G_{12}} - \frac{2\nu_{12}}{E_1}\right)\langle\sin^4\theta\cos^2\theta\rangle \\ &= \frac{1}{E_2} + \left(\frac{1}{G_{12}} - \frac{2\nu_{12}}{E_1} - \frac{2}{E_2}\right)\langle\cos^2\theta\rangle \\ &\quad + \left(\frac{1}{E_1} + \frac{1}{E_2} - \frac{1}{G_{12}} + \frac{2\nu_{12}}{E_1}\right)\langle\cos^4\theta\rangle \end{aligned} \tag{2}$$

where E_1, E_2, and G_{12} are the longitudinal, transverse, and in-plane shear moduli, respectively, and ν_{12} is the Poisson's ratio. Elastic constants and Poisson's ratios for various nanotubes used in this study were obtained from the literatures [111–116] and are listed in Table 3. Due to variation in diameter and chirality, the shear modulus of SWNT bundle depends on its diameter [117]. Shear modulus of the 20 nm diameter bundle was reported to be 1 GPa, while that for the 4.5 nm diameter bundle it was about 6 GPa. Based on the shear modulus of graphite (4.5 GPa) and the geometric packing factor, it was estimated that the shear modulus of nanotubes with homogeneous diameters should approach 19.5 GPa. Values of axial modulus and shear modulus between the planes for MWNTs are based on the reported values

Table 2
Physical carbon nanotube parameters, as well as theoretical and experimental moduli of the various composite fibers

	Diameter (nm)	CNT density (g/cm^3)	CNT (wt%)	CNT (vol%)	PAN/CNT interface area in the composite fiber at 5 wt% loading (m^2/g)	PAN/CNT composite fiber tensile modulus (GPa)	
						Theoretical	Experimental
VGCNF	60	1.95 [116]	5.0	3.1	1.3	9.7	10.6
MWNT	20	1.8 [116]		3.3	5.6	10.7	10.8
SWNT bundle	20	1.3 [112]		4.6	7.7	11.9	–
	10				15.4	–	13.6
	4.5				34.2	21.4	–
DWNT	5	1.5 [5]		4.0	26.6	–	10.8
Exfoliated SWNT	1	1.3 [112]		4.6	154	29.7	–

for graphite [118]. Calculations [119] of axial and shear moduli for various diameter tubes suggest that for 20 nm diameter MWNT tubes, values of E_1 and G_{12} listed in Table 3 based on graphite elastic constants are quite reasonable. Poisson's ratio of 0.14 was also extrapolated based on the calculations reported in reference [119]. Graphite planes in VGCNFs make an angle of 15° to the nano fiber axis [95]. Modulus of VGCNF calculated using Eq. (2) and the misorientation angle of 15°, represents the modulus along the VGCNF axis, which we term as E_{CNT}. Thus axial modulus of VGCNF (E_{CNT}) was determined to be 50 GPa [95]. The effective VGCNF modulus along the composite fiber axis, $(E_{CNT})_{II}$ was estimated to be 44.3 GPa based on the axial VGCNF modulus of 50 GPa and the VGCNF orientation in the composite fiber.

Calculated composite fiber moduli as a function of Herman's orientation factor for various nanotubes are plotted in Fig. 10. Due to the graphite plane misorientation in the VGCNFs, the modulus of the composite fiber is relatively insensitive to the VGCNF orientation, and even at the ideal VGCNF orientation, the modulus of the composite fiber is relatively low. MWNT and SWNT containing fibers exhibit significant modulus dependence on orientation and on SWNT exfoliation. For example, the modulus of the fiber containing 5 wt% MWNT is predicted to be 15 GPa at MWNT orientation of 0.98, while for the ideal MWNT orientation (orientation factor 1), it is predicted to be 34 GPa. This is assuming that the PAN orientation is the same as observed in PAN/MWNT fiber reported in Table 1. However, PAN orientation is also likely to increase with increase in CNT orientation. Therefore, the calculated modulus values in Fig. 10 represent a lower limit. By comparison, calculated modulus of SWNT containing fibers is predicted to be higher, even at lower orientation, provided SWNT bundles are at least partially exfoliated. For example, at SWNT orientation of 0.98, the modulus of the PAN/SWNT composite fiber is predicted to be 21, and 29 GPa for the SWNT bundle diameter values of 4.5, and 1 nm diameters.

Table 3
The elastic constants of SWNTs and MWNTs

	SWNTs			MWNTs
	1 nm	4.5 nm	20 nm	
E_1 (GPa)	640 [112–115]			1060 [118]
E_2 (GPa)	15 [115]			50 [111]
G_{12} (GPa)	19.5 [117]	6 [117]	1 [117]	4 [118]
ν_{12}	0.17 [115]			0.14 [119]

The experimentally observed moduli for SWNT and MWNT containing composite fibers are in excellent agreement with the theoretical values (Table 2). The experimental value of 13.6 GPa for the PAN/SWNT composite is in between the predicted value of 11.9 GPa for 20 nm diameter rope and 21.4 GPa for the 4.5 nm diameter rope. From TEM studies, the rope diameter in the PAN/SWNT composite fiber was estimated to be about 10 nm. The experimental modulus for VGCNF containing composite fiber is somewhat higher than the theoretical values. VGCNF exhibit two types of morphologies, where a second outer layer is composed of highly oriented graphite. The presence of such VGCNF will result in higher observed modulus than the value calculated based on the morphology where all graphite layers are oriented at 15° to the nano fiber axis [95].

In summary, this study clearly shows that polymer/CNT composite fibers can be solution processed using SWNT, DWNT, MWNT, as well as VGCNF. All nanotubes exhibit improvements in tensile, dynamic mechanical, and thermal shrinkage properties and result in higher polymer orientation

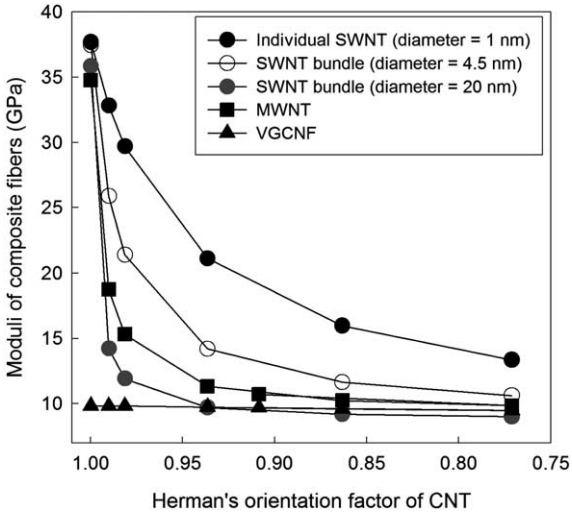

Fig. 10. The calculated tensile modulus of composite fibers containing 5 wt% carbon nanotubes, as a function of carbon nanotube orientation factor, assuming that PAN orientation in the composite fiber is the same as given in the respective composite fibers in Table 1. Points are calculated values, and lines are interpolations.

and crystallite size. The increased polymer orientation and crystal size point to the potential of PAN/CNT composite as the precursor for next generation carbon fiber. Highly entangled DWNTs were most difficult to disperse. All well dispersed nanotubes exhibit high orientation in the drawn composite fiber, while the entangled DWNT globules were unoriented. In the case of PAN/DWNT, poor nanotube dispersion resulted in limited property improvements. While, even the relatively cheaper VGCNF result in useful property gains, the most improvements in properties come from highly dispersed small diameter tubes of long lengths. While the synthesis control can lead to longer nanotubes, they have to be preserved in unentangled state to achieve good dispersion with minimum or no sonication. Achieving ultrahigh nanotube orientation (orientation factor above 0.98) is critical for obtaining high modulus composite fibers containing MWNTs or large diameter SWNT bundles.

Acknowledgements

Financial support for this work from the Office of Naval Research (N00014-01-1-0657), Air Force Office of Scientific Research (F49620-03-1-0124), and Carbon Nanotechnologies, Inc., and the experimental assistance of Marilyn Minus for X-ray diffraction studies are gratefully acknowledged.

References

[1] US Patent 4,565,684; 1986.
[2] Iijima S, Ichihashi T. Nature 1993;363:603–5.
[3] Bethune DS, Kiang CH, Devries MS, Gorman G, Savoy R, Vazquez J, et al. Nature 1993;363:605–7.
[4] Bandow S, Takizawa M, Hirahara K, Yudasaka M, Iijima S. Chem Phys Lett 2001;337:48–54.
[5] Sugai T, Yoshida H, Shimada T, Okazaki T, Shinohara H. Nano Lett 2003;3(6):769–73.
[6] Iijima S. Nature 1991;354:56–8.
[7] Baughman RH, Zakhidov AA, Heer WA. Science 2002;297:787–92.
[8] Thess A, Lee R, Nikolav P, Dai H, Petit P, Robert J, et al. Science 1996; 273:483–7.
[9] Li YL, Kinloch IA, Windle AH. Science 2004;304:276–8.
[10] Ericson LM, Fan H, Peng HQ, Davis VA, Zhou W, Sulpizio J, et al. Science 2004;305:1447–50.
[11] Zhang M, Atkinson KR, Baughman RH. Science 2004;306:1358–61.
[12] Shaffer MSP, Windle AH. Adv Mater 1999;11:937–41.
[13] Zhang X, Liu T, Sreekumar TV, Kumar S, Moore VC, Hauge RH, et al. Nano Lett 2003;3:1285–8.
[14] Cooper CA, Ravich D, Lips D, Mayer J, Wagner HF. Compos Sci Tech 2002;62:1105–12.
[15] Benoit JM, Corraze B, Chauvet O. Phys Rev B 2002;65(24):241405.
[16] Bhattacharrya AR, Sreekumar TV, Liu T, Kumar S, Ericson LM, Hauge RH, et al. Polymer 2003;44:2373–7.
[17] Biercuk MJ, Liaguno MC, Radosavljevic M, Hyun JK, Johnson AT. Appl Phys Lett 2002;80:2767–9.
[18] Kim B, Lee J, Yu I. J Appl Phys 2003;94:6724–8.
[19] Zhang X, Liu T, Sreekumar TV, Kumar S, Hu X, Smith K. Polymer 2004;45:8801–7.
[20] Kumar S, Dang TD, Arnold FE, Bhattacharyya AR, Min BG, Zhang XF, et al. Macromolecules 2002;35:9039–43.
[21] Dalton AV, Collins S, razal J, Munoz E, Ebron VH, Kim BG, et al. J Mater Chem 2004;14:1–3.
[22] Chen J, Hamon MA, Hu H, Chen YS, Rao AM, Eklund PC, et al. Science 1998;282:95–8.
[23] Bahr JL, Yang JP, Kosynkin DV, Bronikowski MJ, Smalley RE, Tour JM. J Am Chem Soc 2001;123:6536–42.
[24] Chen J, Rao AM, Lyuksyutov S, Itkis ME, Hamon MA, Hu H, et al. J Phys Chem B 2001;105:2525–8.
[25] Ramesh S, Ericson LM, Davis VA, Saini RK, Kittrell C, Pasquali M, et al. J Phys Chem B 2004;108:8794–8.
[26] Star A, Liu Y, Grant K, Ridvan L, Stoddart JF, Steuerman DW, et al. Macromolecules 2003;36:553–60.
[27] Peng HQ, Alemany LB, Margrave JL, Khabashesku VN. J Am Chem Soc 2003;125:15174–82.
[28] Niyogi S, Hamon MA, Hu H, Zhao B, Bhowmik P, Sen R, et al. Acc Chem Res 2002;35:1105–13.
[29] Wu M, Shaw LL. J Power Sources 2004;136:37–44.
[30] Mylvaganam K, Zhang LC. J Phys Chem B 2004;108:5217–20.
[31] Clayton LM, Sikder AK, Kumar A, Cinke M, Meyyappan M, Gerasimov TG, et al. Adv Funct Mater 2005;15:101–6.
[32] Sen R, Zhao B, Perea D, Itkis ME, Hu H, Love J, et al. Nano Lett 2004;4: 459–64.
[33] Martin CA, Sandler JKW, Windle AH, Schwarz MK, Bauhoffer W, Schulte K, et al. Polymer 2005;46:877–86.
[34] Pecastaings G, Delhaes P, Derre A, Saadaoui H, Carmona F, Cui S. J Nanosci Nanotechnol 2004;4:838–43.
[35] Zhao B, Hu H, Haddon RC. Adv Funct Mater 2004;14:71–6.
[36] Mrozek RA, Kim BS, Holmberg VC, Taton TA. Nano Lett 2003;3: 1665–9.
[37] Satake A, Miyajima Y, Kobuke Y. Chem Mater 2005;17:716–24.
[38] Sainz R, Benito AM, Martinez MT, Galindo JF, Sotres J, Baro AM, et al. Adv Mater 2005;17:278–81.
[39] An LN, Xu WX, Rajagopalan S, Wang CM, Wang H, Fan Y, et al. Adv Mater 2004;16:2036–40.
[40] Lupo F, Kamalakaran R, Scheu C, Grobert N, Ruhle M. Carbon 2004;42: 1995–9.
[41] Ning JW, Zhang JJ, Pan YB, Guo JK. Mater Sci Eng A 2003;357:392–6.
[42] Laurent C, Peigney A, Rousset A. J Mater Chem 1998;8:1263–72.
[43] Kuzumaki T, Ujiie O, Ichinose H, Ito K. Adv Eng Mater 2000;2:416–8.
[44] Flahaut E, Peigney A, Laurent C, Marliere C, Chastel F, Rousset A. Acta Mater 2000;48:3803–12.
[45] Velasco-Santos C, Martinez-Hernandez AL, Fisher FT, Ruoff R, Castano VM. Chem Mater 2003;15:4470–5.
[46] Thostenson ET, Chou TW. J Phys D 2002;35:L77–L80.
[47] Sreekumar TV, Liu T, Min BG, Guo H, Kumar S, Hauge RH, et al. Adv Mater 2004;16:58–61.
[48] Mamedov AA, Kotov NA, Prato M, Guldi DM, Wicksted JP, Hirsch A. Nature Mater 2002;1:190–4.
[49] Coleman JN, Cadek M, Blake R, Nicolosi V, Ryan KP, Belton C, et al. Adv Funct Mater 2004;14:791–8.
[50] Ma H, Zeng J, Realff ML, Kumar S, Schiraldi DA. Compos Sci Tech 2003;63:1617–28.
[51] Zeng JJ, Saltysiak B, Johnson WS, Schiraldi DA, Kumar S. Compos B 2004;35:245–9.
[52] Kumar S, Doshi H, Srinivasarao M, Park JO, Schiraldi DA. Polymer 2002;43:1701–3.
[53] Ren Y, Fu YQ, Liao K, Li F, Cheng HM. Appl Phys Lett 2004;84: 2811–3.
[54] Pham JQ, Mitchell CA, Bahr JL, Tour JM, Krishanamoorti R, Green PF. J Polym Sci B 2003;41:3339–45.
[55] Gong XY, Liu J, Baskaran S, Voise RD, Young JS. Chem Mater 2000; 12:1049–52.
[56] Baek JB, Lyons CB, Tan LS. Macromolecules 2004;37:8278–85.
[57] Grunlan JC, Mehrabi AR, Bannon MV, Bahr JL. Adv Mater 2004;16: 150–3.
[58] Sandler JKW, Kirk JE, Kinloch IA, Shaffer MSP, Windle AH. Polymer 2003;44:5893–9.
[59] Shenogin S, Xue LP, Ozisik R, Keblinski P, Cahill DG. J Appl Phys 2004;95:8136–44.

[60] Guo H, Sreekumar TV, Liu T, Marylin M, Kumar S. Polymer 2005; 46(9):3001–5.
[61] Potschke P, Fornes TD, Paul DR. Polymer 2002;43:3247–55.
[62] Liu T, Sreekumar TV, Kumar S, Hauge RH, Smalley RE. Carbon 2003; 41:2427–51.
[63] Kymakis E, Alexandrou I, Amaratunga GAJ. J Appl Phys 2003;93: 1764–8.
[64] Xiao QF, Zhou X. Electrochim Acta 2003;48:575–80.
[65] Wang QH, Setlur AA, Lauerhaas JM, Dai JY, Seelig EW, Chang RPH. Appl Phys Lett 1998;72:2912–3.
[66] Kim JY, Kim M, Choi JH. Synth Met 2003;139:565–8.
[67] Park JH, Choi JH, Moon JS, Kushinov DG, Yoo JB, Park CY, et al. Carbon 2005;43:698–703.
[68] Sayago I, Terrado E, Lafuente E, Horrillo MC, Maser WK, Benito AM, et al. Synth Met 2005;148:15–19.
[69] Abraham JK, Philip B, Witchurch A, Varadan VK, Reddy CC. Smart Mater Struct 2004;13:1045–9.
[70] Zhao Q, Frogley MD, Wagner HD. Polym Adv Tech 2002;13:759–64.
[71] Wood JR, Zhao Q, Frogley MD, Meurs ER, Prins AD, Peijs T, et al. Phys Rev B 2000;62:7571–5.
[72] Raravikar NR, Keblinski P, Rao AM, Dresselhaus MS, Schadler LS, Ajayan PM. Phys Rev B 2002;66:235424.
[73] Wang H, Zhou W, Ho DL, Winey KI, Fischer JE, Glinka CJ, et al. Nano Lett 2004;4:1789–93.
[74] Matarredona O, Rhoads H, Li ZR, Harwell JH, Balzano L, Resasco DE. J Phys Chem B 2003;107:13357–67.
[75] Potschke P, Bhattacharyya AR, Janke A. Eur Polym J 2004;40:137–48.
[76] Cadek M, Coleman JN, Barron V, Hedicke K, Blau WJ. Appl Phys Lett 2002;81:5123–5.
[77] Jin Z, Pramoda KP, Xu G, Goh SH. Chem Phys Lett 2001;337:43–7.
[78] Schadler LS, Giannaris SC, Ajayan PM. Appl Phys Lett 1998;73: 3842–4.
[79] Gojny FH, Wichmann MHG, Kopke U, Fiedler B, Schulte K. Compos Sci Tech 2004;64:2363–71.
[80] Pirlot C, Willems I, Fonseca A, Nagy JB, Delhalle J. Adv Eng Mater 2002;4:109–14.
[81] Pirlot C, Mekhalif Z, Fonseca A, Nagy JB, Demortier G, Delhalle J. Chem Phys Lett 2003;372:595–602.
[82] Weisenberger MC, Grulke EA, Jacques D, Rantell T, Andrews R. J Nanosci Nanotech 2003;3:535–9.
[83] Ye HH, Lam H, Titchenal N, Gogotsi Y, Ko F. Appl Phys Lett 2004;85: 1775–7.
[84] Ge JJ, Hou H, Li Q, Graham MJ, Greiner A, Reneker DH, et al. J Am Chem Soc 2004;126:15754–61.
[85] Ko F, Gogotsi Y, Ali A, Naguib N, Ye HH, Yang GL, et al. Adv Mater 2003;15(14):1161–5.
[86] Min BG, Sreekumar TV, Uchida T, Kumar S. Carbon 2005;43(3): 599–604.
[87] Koganemaru A, Bin Y, Agari Y, Matsuo M. Adv Funct Mater 2004; 14(9):842–50.
[88] Kim SH, Min BG, Lee SC, Park SB, Lee TD, Park M, et al. Fibers Polym 2004;5:198–203.
[89] Wang B, Li JW, Wang HP, Jiang JM, Liu YQ. Macromol Symp 2004; 216:189–94.
[90] Masson JC. Acrylic fiber technology and applications. New York: Marcel Dekker; 1995.
[91] Bahl OP, Shen Z, Lavin JG, Ross RA. In: Donnet JB, Wang TK, Rebouillat S, Peng JCM, editors. Carbon fibers. New York: Marcel Dekker; 1998. p. 1–84.
[92] Cadek M, Coleman JN, Ryan KP, Nicolosi V, Bister G, Fonseca A, et al. Nano Lett 2004;4(2):353–6.
[93] Chiang IW, Brinson BE, Smalley RE, Margrave JL, Hauge RH. J Phys Chem B 2001;105:1157–61.
[94] Liu T, Kumar S. Chem Phys Lett 2003;378:257–62.
[95] Uchida T, Anderson DP, Minus ML, Kumar S. J Mater Sci; in press.
[96] Hobson RJ, Windle AH. Macromolecules 1993;26:6903–7.
[97] Yamane A, Sawai D, Kameda T, Kanamoto T, Ito M, Porter RS. Macromolecules 1997;30:4170–8.
[98] Sawai D, Yamane A, Kameda T, Kanamoto T, Ito M, Yamazaki H, et al. Macromolecules 1999;32:5622–30.
[99] Cullity BD. Elements of X-ray diffraction. 2nd ed. Reading, MA: Addison-Wesley Publishing Company; 1978 p. 102.
[100] Shimamura K, Minter JR, Thomas EL. J Mater Sci Lett 1983;18: 54–8.
[101] Donald AM, Windle AH. In: Cahn RW, Davis EA, Ward IM, editors. Liquid crystalline polymers. Cambridge: Cambridge University Press; 1992. p. 250.
[102] Zimmerman J, Kohan MI. J Polym Sci A 2001;39:2565–70.
[103] Luo S, Grubb DT, Netravali AN. Polymer 2002;43:4159–66.
[104] Ledbetter HD, Rosenberg S, Hurtig CW. Mater Res Soc Symp Proc 1989;134:253–64.
[105] Uchida T, Kumar S. J Appl Polym Sci 2005;98(3):985–9.
[106] Endo M, Kim YA, Hayashi T, Yangisawa T, Muramatsu H, Ezaka M, et al. Carbon 2003;41:1941–7.
[107] Hamon MA, Itkis ME, Niyogi S, Alvarez T, Kuper C, Menon M, et al. J Am Chem Soc 2001;123:11292–3.
[108] Dumitrica T, Landis CM, Yakobson BI. Chem Phys Lett 2002;360: 182–8.
[109] Liu T, Kumar S. Nano Lett 2003;3:647–50.
[110] Ward IM, Hadley DW. An introduction to the mechanical properties of solid polymers. New York: Wiley; 1995 p. 300 [reprinted].
[111] Koerner H, Liu W, Alexander M, Mirau P, Dowty H, Vaia RA. Polymer 2005;46(12):4405–20.
[112] Lu JP. Phys Rev Lett 1997;79:1297–300.
[113] Gao GH, Cagin T, Goddard WA. Nanotechnology 1998;9:184–91.
[114] Sinnott SB, Shenderova OA, White CT, Brenner DW. Carbon 1998; 36:1–9.
[115] Popov VN, Van Doren VE, Balkanski M. Solid State Commun 2000; 114:395–9.
[116] Provided by the manufacturer.
[117] Salvetat JP, Briggs GAD, Bonard JM, Bacsa RR, Kulik AJ, Stockli T, et al. Phys Rev Lett 1999;82:944–7.
[118] Johnson W. The structure of PAN based carbon fibers and relationship to the physical properties. In: Watt W, Perov BV, editors. Handbook of composites. Strong fibers, vol. 1. New York: Elsevier Sicence Publisher; 1988. p. 393.
[119] Shen L, Li J. Phys Rev B 2005;71:035412.